Laser surface melting of Ti–10V–2Fe–3Al alloy

J. H. ABBOUD, D. R. F. WEST
Department of Materials, Imperial College of Science, Technology and Medicine, London SW7 2BP, UK

Laser surface melting of Ti and Ti alloys has been used to obtain rapid solidification with resultant fine-scale microstructures and segregation [1, 2]. For example, laser surface melting of α-Ti (e.g. commercial purity Ti; Ti–5.5Al–3.5Sn–1Nb–0.3Si) and $(\alpha + \beta)$-Ti (e.g. Ti–6Al–4V) has been carried out using a 2 kW c.w. CO_2 laser [1]. The results showed the expected decrease in width and depth of the melted zone with increasing traverse speed; the microstructure was martensite. Laser surface melting of β-Ti alloy leads to the formation of cellular/dendritic microstructures (see, for example [3]); the cell/dendrite spacings decrease with increasing traverse speed (e.g. increasing cooling rates). Work on laser surface melting of Ti–15V–3Cr–3Al–3Sn alloy has been carried out by Peng *et al.* [3], leading to an equation to correlate the cooling rate $(\dot{T}, K\ s^{-1})$ with cell/dendrite spacings $(d, \mu m)$ using a heat transfer model.

$$d = 80\dot{T}^{-0.34}$$

This equation is similar to that in previous work by Narminen and Brody [4] but with differences in the coefficients. Because of the epitaxial growth from the β-grains in the heat-affected zone (HAZ), the β-grain size in the melted zone was coarse with a columnar morphology. Folkes [2] and Abboud *et al.* [5] carried out laser surface melting of Ti–15 wt% Mo alloy using a range of traverse speeds and powers [5]. The results showed a decrease in the cell/dendrite spacing from 7.5 μm at 5 mm s^{-1} to about 1 μm at 300 mm s^{-1}. A mathematical model based on heat transfer theory was used to calculate the cooling rates. The results showed a good agreement between the calculated values and the values obtained from the Peng equation. Laser surface melting of Ti–22Fe, Ti–40W, Ti–9Co and Ti–5.5Ni (wt%) alloys has been investigated using powers from 300 to 600 W [6, 7]. The microstructures in the first three alloys were single-phase β, whereas Ti–5.5Ni consisted of proeutectoid α and eutectoid consisting of $\alpha + Ti_2Ni$ with an interphase spacing of approximately 100 nm. The process of laser surface melting has been developed to include a compositional change by the addition of other elements into the laser-melted zone in order to modify the surface properties such as hardness, and resistance to erosion and corrosion. For instance, preplacing carbon on the surface of Ti substrates

followed by laser melting can be used to produce TiC dendrites in a martensitic (α') matrix with an average hardness level of about 600 H_v [8]. Similarly, TiN dendrites in an α/α' matrix can be produced by laser melting of Ti substrates in atmospheres containing nitrogen [8].

Recently, investigations have been reported of laser surface alloying of commercial purity Ti with Al or Si, using a powder feeding technique, to produce titanium aluminides or titanium silicides, respectively [9, 10]. The results show that by the proper selection of laser processing parameters and powder feed rates, rapidly solidified Ti–Al or Ti–Si alloyed layers over a wide range of compositions can be produced. The injection of SiC particles into the laser-melted zone of commercial purity Ti and Ti–6Al–4V alloy has also been explored [11, 12]. The reaction between the SiC particles and the molten Ti leads to the formation of TiC dendrites, eutectic consisting of α/α'-Ti + Ti_5Si_3 and martensite; the matrix hardness was increased from about 200 to about 600 H_v. Currently, an investigation is in progress of laser surface melting/particle injection of commercial purity Ti and β-Ti (Ti–10V–2Fe–3Al) alloy using a continuous feed of ceramic (SiC and TiB_2) into a melted pool produced by high-power c.w. CO_2 lasers.

This letter reports some preliminary results of laser surface melting of Ti–10V–2Fe–3Al (Ti–10–2–3) alloy at different power levels, including some microstructural study of the alloy before and after laser melting.

Table I shows the composition and Fig. 1 shows the microstructure of the Ti–10–2–3 alloy, which was received in the form of plate of about 10 mm thickness. A 2 kW and a 5 kW c.w. CO_2 laser, operated at 3 and 5 mm beam diameter, respectively, were used for laser surface melting. The traverse speeds between the substrate and the laser beam were 8.1 and 10 mm s^{-1}. After laser melting, samples were cut transversely through the melted zone, and standard methods were used for metallographic observations and X-ray diffraction. Thin foils were prepared by cutting a slice 1 mm thick, parallel to the laser-melted zone; each slice was ground down to approximately 300 μm thickness. Discs 3 mm in diameter were cut by spark erosion and were ground down to approximately 100 μm thickness. Electropolishing was carried out using a

TABLE I Chemical composition of the Ti–10–2–3 alloy (wt%)

Ti	V	Fe	Al	O	N	H	C	B	Mo	Sn	Mn	Y
Balance	9.9	1.8	3.0	0.1	0.006	0.005	0.001	0.001	0.008	0.01	0.001	<0.01
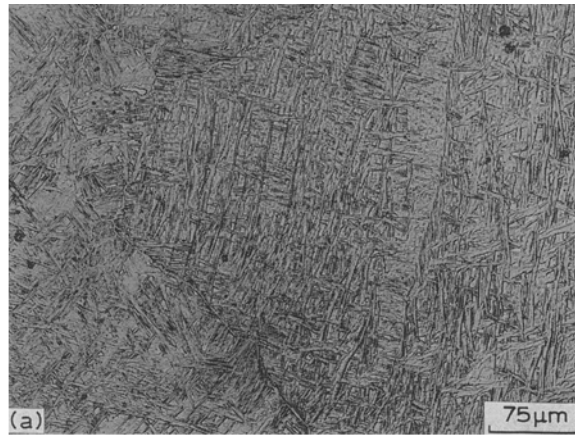
Figure 1 Microstructure of the Ti–10–2–3 alloy as-received: (a) optical microscopy and (b) TEM bright-field micrograph.

showed that two phases were present, namely $\alpha + \beta$ (Table III).

Fig. 2a shows a transverse section of the Ti–10–2–3 alloy melted zone as processed at 1.6 kW power, 3 mm beam diameter and 10 mm s^{-1} traverse speed. The structure is predominantly coarse β grains of width about 0.1–0.3 mm grown epitaxially from the HAZ. Within these grains are alternate light and dark areas forming a cellular structure (Fig. 2b) with average cell spacing of about 10 μm suggesting a cooling rate of the order of 10^3 K s^{-1} [3]. Observations of the melted zone by optical microscopy revealed acicular features interpreted as plates of the orthorhombic martensite phase (α''); the bands of martensite were aligned along the cell axes and appear to lie within the cells, rather than the intercell regions. EDAX compositional analysis, in the β region and the martensite features, showed slightly lower V and Fe contents in the regions of ($\alpha'' + \beta$) than in the β regions, as shown in Table IV. This is consistent with a "coring" effect associated with non-equilibrium solidification. The M_S temperature of the Ti–10–2–3 alloy has been reported to be close to room temperature [13]; the slightly lower V and Fe contents in the regions first to solidify, resulting from coring, raises the M_S temperature and favours martensite formation.

Examination of the upper surface of the melted

solution containing 5 vol% H_2SO_4 in methanol. Microanalysis was carried out by transmission electron microscopy (TEM) provided with energy-dispersive X-ray analysis (EDAX).

The as-received alloy was treated within the ($\alpha + \beta$) region to produce a structure consisting essentially of α + retained β; the phase compositions as determined by scanning TEM (STEM; Table II) showed partitioning of V and Fe to β and Al to α, consistent with data from previous work on a Ti–10–2–3 alloy [6]. X-ray diffraction analysis

TABLE II STEM analysis of the as-received Ti–10–2–3 alloy (wt%)

Phase	Ti	V	Fe	Al
α	Balance	2.4 ± 0.2	0.1 ± 0.2	3.6 ± 0.2
β	Balance	21.0 ± 0.2	4.0 ± 0.2	1.5 ± 0.2

TABLE IV EDAX compositional analysis (wt%) of the laser surface melted region of Ti–10–2–3 alloy processed at 1.6 kW power, 10 mm s^{-1} traverse speed and 3 mm beam diameter

Phase	Ti	V	Fe	Al
α	Balance	10.5	2.0	2.8
$\alpha'' + \beta$	Balance	9.9	1.20	3.0

TABLE III X-ray diffraction data of the as-received Ti–10–2–3 alloy and after laser melting, 4.5 kW power, 8.1 mm s^{-1} speed and 5 mm beam diameter

As-received			Laser-melted			
Diffraction angle, 2θ (degrees)	d-spacing (nm)	$h\,k\,l$	2θ (degrees)	d (nm)	$h\,k\,l$	Intensity[a]
35.4	2.53	$(0\,1\,\bar{1}\,0)_\alpha$				s
38.6	2.33	$(0\,0\,0\,2)_\alpha$				s
39.9	2.26	$(1\,1\,0)_\beta$	39.3	2.29	$(1\,1\,0)_\beta$	vs
40.5	2.22	$(0\,1\,\bar{1}\,1)_\alpha$				vs
53.4	1.72	$(0\,1\,\bar{1}\,2)_\alpha$				m
57.6	1.60	$(2\,0\,0)_\beta$	57.0	1.61	$(2\,0\,0)_\beta$	w
63.5	1.46	$(1\,1\,\bar{2}\,0)_\alpha$				m
71.0	1.32	$(2\,1\,1)_\beta$	71.2	1.32	$(2\,1\,1)_\beta$	s
72.4	1.30	$(1\,0\,\bar{1}\,3)_\alpha$				m
76.8	1.24	$(1\,1\,\bar{2}\,2)_\alpha$				m
78.0	1.22	$(2\,0\,\bar{2}\,1)_\alpha$				m

[a]vs, Very strong; s, strong; m, medium; w, weak.

zone (as processed) showed a rippling effect typical of laser-melted metals (Fig. 2c) with uniform ripple size and spacing; in some areas columnar grain growth in the direction of traverse occurred. After polishing and etching of the upper surface, marten-

site plates were observed within regions following the ripple pattern (Fig. 2d); these may result from a segregation mechanism related to the rippling, giving rise to regions depleted in V and Fe.

Transverse sections of the laser-melted zones
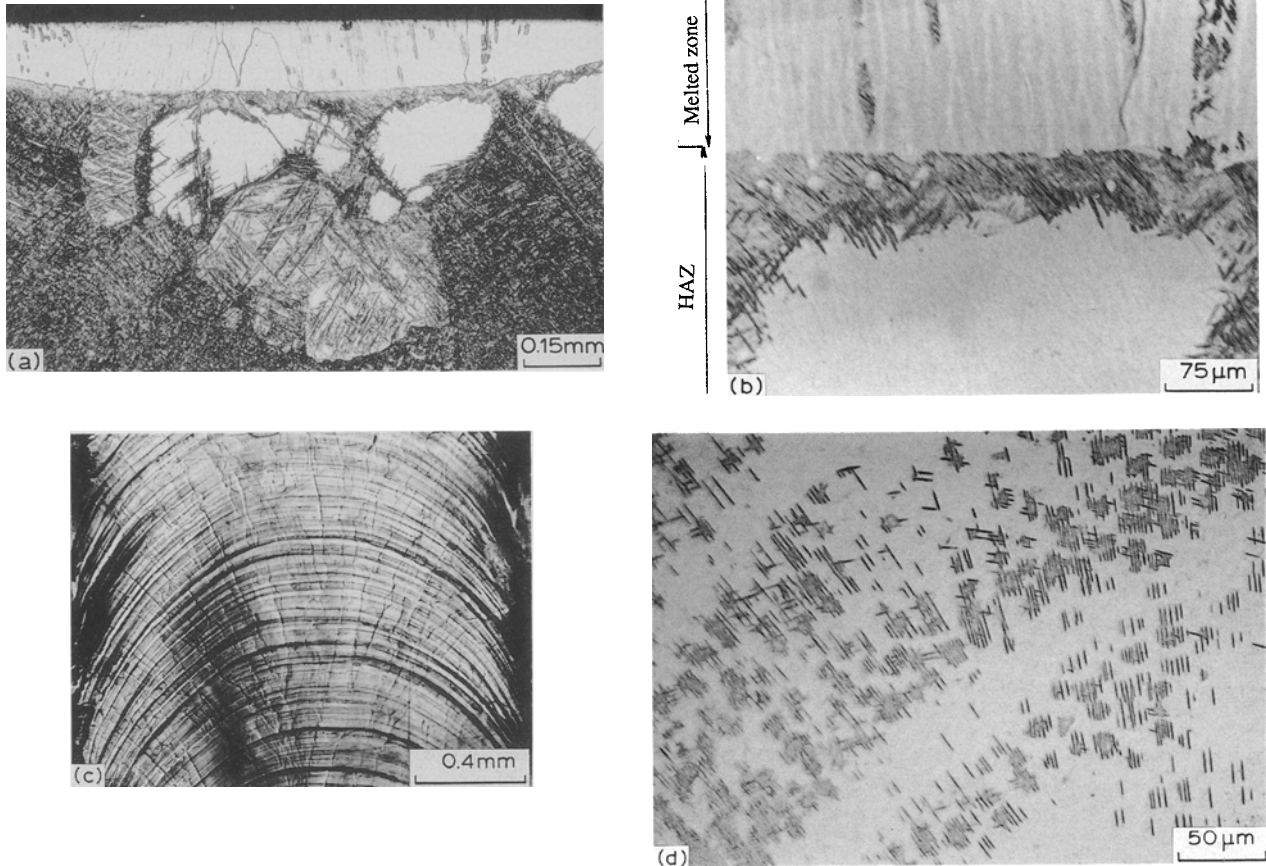
Figure 2 Optical micrographs showing the microstructure of the laser-melted zone of Ti–10–2–3 alloy processed at 1.6 kW, 3 mm and 10 mm s^{-1}: (a) transverse section, (b) interface between the laser-melted zone and the HAZ, (c) Top surface view showing rippling and (d) orthorhombic martensite ($\alpha'' + \beta$).

Figure 3 Optical micrographs showing transverse sections of laser-melted zones processed at 5 mm beam diameter, 8.1 mm s^{-1} traverse speed and power (a) 3.5 kW, (b) 4 kW and (c) 4.5 kW.

1324

corresponding to power levels of 3.5, 4 and 4.5 kW, respectively, at 5 mm beam diameter and 8.1 mm s^{-1} traverse speed are shown in Fig. 3a–c. The width and the depth of the zone increased with increasing specific energy (P/DV, where P is the laser power, D is the beam diameter and V is the traverse speed), as expected (Figs 3 and 4) and the cell spacing showed a small increase with increasing power, which is consistent with the decrease in cooling rate associated with increased dimensions of the melted zone.

In the HAZ, which extended to a distance equal to approximately the depth of the melted zone for the specimens processed at 3.5–4.5 kW, the original ($\alpha + \beta$) structure had transformed to β; upon cooling the β had partially transformed to an acicular product interpreted as orthorhombic martensite (α''; Fig. 3). Martensite formation occurred preferentially at β grain boundaries and at the melted zone–HAZ interface. The extent to which martensite formed varied considerably among the various processing conditions. For example, in the specimen processed at 4.5 kW β retention was virtually complete, whereas at 3.5 and 4 kW substantial proportions of martensite formed. The importance of the interfaces suggested that nucleation may be aided by local stress effects raising M_S. It is also probable that local solute concentration gradients may exist within the HAZ, due to the heating cycle being too short to allow complete homogenization of the β during the ($\alpha + \beta$) $\rightarrow$ β transformation.

The melted zone of the sample processed at 4.5 kW (Fig. 3c) as examined by TEM showed that β-phase is featureless (apart from dislocations; Fig. 5a); some martensite plates were also observed (Fig. 5b). Diffraction analysis of the β-phase showed the presence of ω-phase (Fig. 5c). STEM analysis of the β-phase showed uniform composition, whereas in the regions of martensite $+$ β there was a depletion of V and Fe (Table V). This observation is consistent with the coring effect shown by EDAX in the bulk sample.
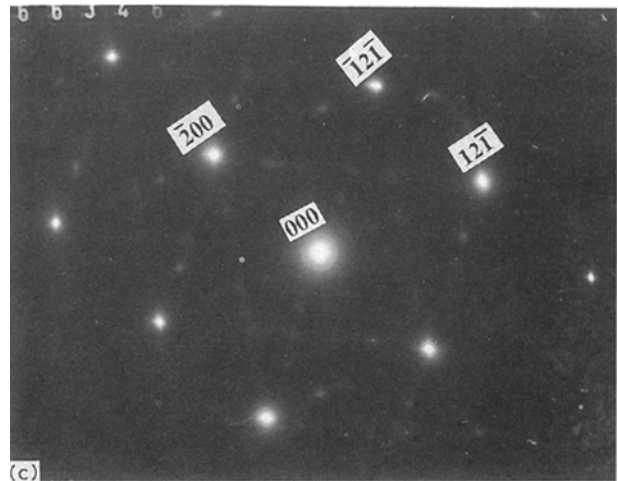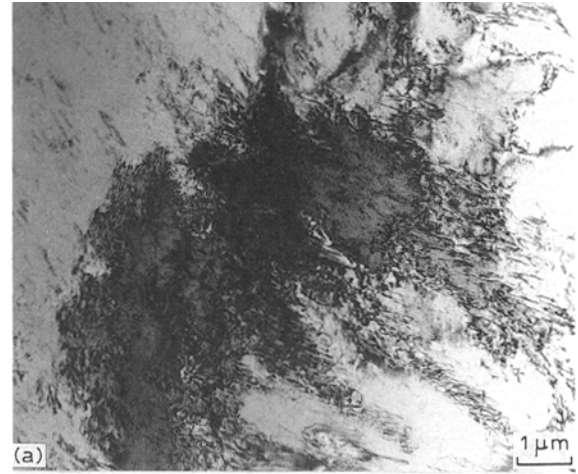
Figure 5 Microstructure of the laser-melted zone processed at 4.5 kW, 5 mm and 8.1 mm s^{-1}: (a) TEM bright-field micrograph showing β-phase, (b) TEM bright-field micrograph showing ($\alpha'' + \beta$) and (c) diffraction pattern of β-phase showing ω-phase, zone axis [0 1 2]$_\beta$.

TABLE V STEM analysis (wt %) of the laser surface melted region of Ti–10–2–3 alloy processed at 4.5 kW laser power, 8.1 mm s^{-1} traverse speed and 5 mm beam diameter

Phase	Ti	V	Fe	Al
α	Balance	10 $\pm$ 0.4	1.5 $\pm$ 0.2	2.9 $\pm$ 0.2
$\alpha'' + \beta$	Balance	8.9 $\pm$ 0.4	1.0 $\pm$ 0.2	2.8 $\pm$ 0.2

Figure 4 Variation of melt zone dimensions with specific energy (P/DV), where P is the laser power, D is the beam diameter and V is the traverse speed. (○) Depth D and (●) width W.

Acknowledgements

References

1. A. S. UBHI, T. N. BAKER, P. HOLDWAY and A. W. BOWEN, in Sixth International Conference on the Processing of Titanium, Cannes, June 1988, Pt III, edited by P. G. Lacombe, R. Tricot and (Societe Francaise de Metallurgie, 1988) Beranjer p. 1613.
2. J. FOLKES, PhD thesis, Imperial College, University of London (1986).
3. T. C. PENG, S. M. SASTRY, J. E. O'NEAL and J. F. TESSON, in Lasers in Materials Processing, Conference Proceedings, edited by E. A. Metzbower (American Society for Metals, Metals Park, Ohio, 1983) p. 241.
4. J. I. NARMINEN and J. D. BRODY, in "Titanium, science, and technology", edited by R. I. Jaffee and H. M. Burts, Vol. 3 (Plenum Press, New York, 1973) p. 1893.
5. J. H. ABBOUD, W. M. STEEN and D. R. F. WEST, Unpublished work (1989).
6. W. A. BAESLACK, I. WEETER, S. KRISHNA-MURTHY, P. SMITH and F. H. FROES, in Materials Research Society, Symposium Proceedings, edited by B. H. Kear, Vol. 28 (North-Holland, Amsterdam, 1984) p. 375.
7. Idem, in "Titanium rapid solidification technology", edited by F. H. Froes and D. Eylon (TMS-AIME, Warrendale, PA, 1986) p. 97.
8. A. WALKER, J. FOLKES, W. M. STEEN and D. R. F. WEST, Surf. Engng 1 (1985) 23.
9. J. H. ABBOUD and D. R. F. WEST, Mater. Sci. Technol. 7 (1991) 353.
10. Idem, Surf. Engng 7 (1991) 159.
11. Idem, Mater. Sci. Technol. 5 (1989) 725.
12. Idem, J. Mater. Sci. Lett. 10 (1991) 1149.
13. A. I. P. NWOBU, H. M. FLOWER and D. R. F. WEST, Mater. Sci. Technol. 7 (1991) 391.